The Effect of Organoclay on the Mechanical Properties and Morphology of Injection-Molded Polyamide 6/Polypropylene Nanocomposites

W. S. Chow,[1] Z. A. Mohd. Ishak,[1] U. S. Ishiaku,[2] J. Karger-Kocsis,[3] A. A. Apostolov[4]

[1]*School of Materials and Mineral Resources Engineering, Engineering Campus, Universiti Sains Malaysia, Seri Ampangan, 14300 Nibong Tebal, Penang, Malaysia*
[2]*Advanced Fibro-Science, Kyoto Institute of Technology, Matsugasaki, Sakyo-ku, Kyoto 606-8585, Japan*
[3]*Institute for Composite Materials Ltd., University of Kaiserslautern, P.O. Box 3049, D-67663 Kaiserslautern, Germany*
[4]*Laboratory on Structure and Properties of Polymers, Sofia University, BG-1126 Sofia, Bulgaria*

Received 8 January 2003; accepted 16 April 2003

ABSTRACT: Nanocomposites containing a thermoplastic blend and organophilic layered clay (organoclay) were produced by melt compounding. The blend composition was kept constant [polyamide 6 (PA6) 70 wt % + polypropylene (PP) 30 wt %], whereas the organoclay content was varied between 0 and 10 wt %. The mechanical properties of the nanocomposites were determined on injection-molded specimens in both tensile and flexural loading. Highest strength values were observed at an organoclay content of 4 wt % for the blends. The flexural strength was superior to the tensile one, which was traced to the effect of the molding-induced skin-core structure. Increasing organoclay amount resulted in severe material embrittlement reflected in a drop of both strength and strain values. The morphology of the nanocomposites was studied by scanning electron microscopy (SEM), transmission electron microscopy (TEM), energy-dispersion X-ray analysis (EDX), and X-ray diffraction (XRD). It was established that the organoclay is well dispersed (exfoliated) and preferentially embedded in the PA6 phase. Further, the exfoliation degree of the organoclay decreased with increasing organoclay content. © 2003 Wiley Periodicals, Inc. J Appl Polym Sci 91: 175–189, 2004

Key words: polyamide; polypropylene; organoclay; nanocomposite

INTRODUCTION

Nanocomposites offer new technological and economical benefits. The incorporation of nanometer scale reinforcement (e.g., layered silicates of clay, nanofiber, nanotubes, and metal nanoparticles in polymeric materials) may dramatically improve selected properties of the related polymer. Polymer nanocomposites with layered silicates represent a hybrid between organic and inorganic materials.[1] Naturally occurring montmorillonite is the most abundant member of the smectite family of clays. Naturally occurring montmorillonite is incompatible with most polymers because of its hydrophilic nature. Ion exchange is widely practiced to modify the montmorillonite's surface to increase its compatibility with mostly hydrophobic polymer.[2]

Melt intercalation of inorganic clay mineral consisting of layered silicates with polymers is a viable approach to prepare a variety of polymer–clay nanocomposites. These nanocomposites exhibit superior properties such as enhanced strength, reduced gas permeability, and improved flame retardancy.[3] Direct polymer melt intercalation is the most attractive method because of its low cost, high output, and applicability of current polymer processing techniques.[4] Numerous researchers described polymer–clay nanocomposites on the basis of single-polymer matrix, including polypropylene (PP)[5–10], polyamide (PA)[11–15], polystyrene,[16–18] polyimide (PI)[19–21], epoxy,[22–24] poly(methyl methacrylate),[25–26] unsaturated polyester,[27] polycaprolactone,[28] poly(ethylene oxide),[29] and polycarbonate.[30] However, thermoplastic nanocomposites based on blends of two or more polymers (i.e., binary blends or ternary blends of thermoplastics) were less involved in studies according to the open literature. The present research focuses on the polymer melt intercalation method to produce PA6/PP binary blend based nanocomposites.

PA6 and PP blending was attempted to achieve improvement in mechanical properties, paintability, and barrier properties.[31] PA6 has good barrier against oxygen, but shows poor resistance to water and water vapor. On the contrary, PP exhibits excellent moisture barrier but poor oxygen barrier properties. The presence of impermeable silicate layers in a polymeric

Correspondence to: Z. A. M. Ishak (zarifin@eng.usm.my).
Contract grant sponsor: Ministry of Science, Technology, and Environment (MOSTE), Malaysia; contract grant number: 063171/IRPA.

Journal of Applied Polymer Science, Vol. 91, 175–189 (2004)

matrix may increase the resistance to both water and gas permeation.[32] The present study is devoted to the study of the effects of organoclay on the mechanical properties of PA6/PP blend based nanocomposites. A PA6 dominant blend was chosen because of its good compatibility with the octadecylamine-modified organoclay used in this study. A minor portion of PP (30 wt %) was added into the PA6 matrix with the aim of improving the water barrier properties of PA6. Attention was paid to clarify the effects of organoclay loading (0–10 wt %) on the mechanical properties and morphology of the PA6/PP (70/30 wt %) blend.

EXPERIMENTAL

Materials

The PA6 (Amilan CM 1017) used in this study was a commercial product from Toray Nylon Resin Amilan (Japan). Melt flow index (MFI) and density of PA6 were 35 g/10 min (at 230°C and 2.16 kg load) and 1.14 g/cm^3, respectively. PP (Pro-Fax SM-240) was supplied by Titan Himont Polymer (M) Sdn. Bhd. (Malaysia). MFI and density of PP is 25 g/10 min (at 230°C and 2.16 kg load) and 0.9 g/cm^3, respectively. Organoclay (1.30TC Nanomer) was a commercial product from Nanocor, Inc. (USA). The organoclay is a white powder containing montmorillonite clay (70–85 wt %) intercalated by octadecylamine (15–30 wt %). The mean dry particle size of organoclay was between 16 and 22 μm.

Compounding

Melt compounding of the PA6/PP (70/30) blends and nanocomposites was done on a counterrotating twin-screw extruder (Haake Rheodrive 3000). The extrusion zone temperature ranged from 220 to 230°C. Prior to extrusion, PA6 pellets and organoclay were dehumidified by using a vacuum oven at 80°C for 8 h. The extrudates were pelletized with the Haake pelletizer.

Injection molding

The pellets were injection molded into a standard tensile bar by using a Niigata AN 50 injection-molding machine. Injection molding temperature ranged from 225 to 240°C. Prior to injection molding, all pellets were dehumidified by using a vacuum oven at 80°C for 8 h.

Mechanical properties

Tensile and flexural testing were done according ASTM D638 and ASTM D790, respectively, by using an Instron 5582 machine. The deformation rate was set for 50 and 3 mm/min for tensile and flexural testing, respectively.

Morphology study

Fracture surface morphology studies of selected PA6/PP blend nanocomposites were analyzed by using scanning electron microscopy (SEM, model S 360, Leica Cambridge Ltd.). The fracture surface was gold coated to avoid electrostatic charging during inspection.

X-ray diffraction (XRD)

XRD measurements were done with a D500 diffractometer (Siemens, Germany) with Ni-filtered CuKα radiation. A special set of blends dropped to $2\theta = 0.4°$ (which corresponds to an interlayer spacing of 22 nm). The samples were scanned in reflection in the interval $2\theta = 0.4–10°$. The interlayer spacing of the organoclay was calculated from the related peak position (d_{001}-reflection) in the XRD diffractogram.

Transmission electron microscopy (TEM)

TEM measurements were carried out with a LEO 912 Omega transmission electron microscope applying an acceleration voltage of 120 keV. The specimens were prepared by using an Ultracut E (Reichert and Jung) ultramicrotome. Thin sections of about 100 nm thickness were cut with a Diatome diamond knife at room temperature.

RESULTS AND DISCUSSION

Melt flow index

Effect of blend composition

Figure 1 compares the experimental and calculated MFI (supposing that the rule of mixture holds) values for the PA6/PP blends at different blending ratios. Blending of PA6 and PP yielded a positive deviation in the MFI in respect to the additive rule. Recall that the MFI is the reciprocal value of the viscosity. Thus, the viscosity of the PA6/PP blends shows a negative deviation from the rule of mixture. This indicates that PA6 and PP are not compatible with each other.

Ide and Hasegawa[33] have noted that the MFI of mechanically blended PA6/PP increased proportionally with the PA6 content. There was little interaction between PA6 and PP. According to Liang et al., from the viscosity-composition plot for PA6/PP blends, the viscosity of PA6/PP (75/25) at shear rates 10^1,10^2, and 10^3 s^{-1} is lower than PA6.[34] This means that the MFI of the PA6/PP (75/25 wt %) blend was higher than the plain PA6. Blend properties may exhibit either positive or negative deviation from additivity.[35] Accord-

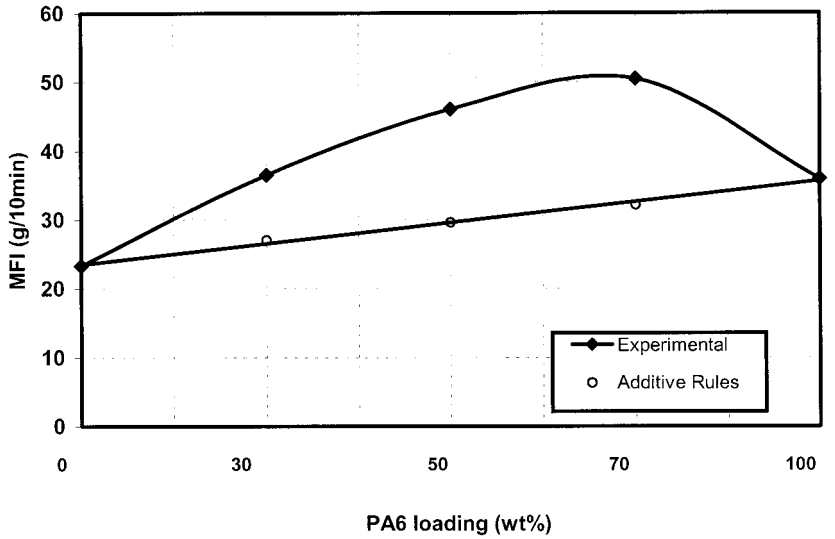

Figure 1 Comparison between the experimental and additivity rule calculated MFI values as a function of blend formulation.

ing to Marco et al., the flow behavior of noncompatibilized PP/PA6 blends is in between those of the pure components and represents a negative deviation from the additive rule over the composition range analyzed. This suggests a bad adhesion between the PA6 and PP phase and thus a high level of incompatibility.[36] According to Park et al.[37] and Robson et al.,[38] for all shear rates tested, the viscosity of the PA6/PP blend shows negative deviation from the simple additive rule, which indicates the incompatibility of the blend.

Effect of organoclay loading

Figure 2 shows the effect of organoclay on the MFI of PA6/PP-based composites. The MFI decreased with increasing organoclay content, which may be attributed to the interaction between the organoclay and the PA6. There may be some chemical interaction between organoclay and PA6, due to the amine groups of the intercalant (modifier) in the organoclay and amide, amine and carboxyl groups in the PA6. This interaction is believed to be responsible for the decrease of the MFI.

Density

Table I shows the densities of neat PA6, PP, PA6/PP blends and organoclay-filled PA6/PP nanocomposites. The densities of all PA6/PP blends and nanocomposites are lower than the density of neat PA6. How-

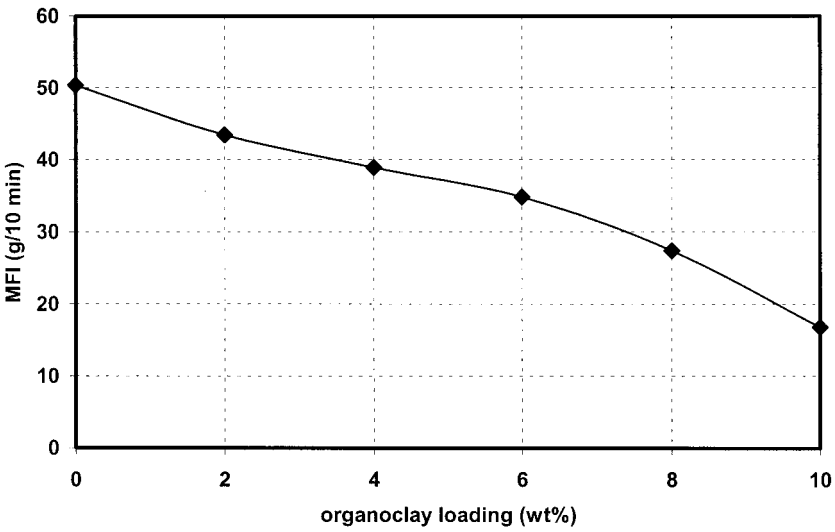

Figure 2 Effect of organoclay content on the MFI.

TABLE I
Density of Neat PA6, PP, PA6/PP Blends and Organoclay-Filled PA6/PP Nanocomposites

Material	Density (g/cm^3)
PA6	1.12
PP	0.90
PA6/PP	0.95
PA6/PP/2 wt % organoclay	1.02
PA6/PP/4 wt % organoclay	1.03
PA6/PP/6 wt % organoclay	1.03
PA6/PP/8 wt % organoclay	1.04
PA6/PP/10 wt % organoclay	1.05

ever, the incorporation of organoclay has slightly increased the density of PA6/PP-based composites.

Mechanical properties

Effect of blend composition

The effect of PA6 and PP blending on the Young's modulus and yield stress is shown in Figure 3. As expected, the addition of 30 wt % of PP reduces the tensile modulus of PA6. This is in agreement with an earlier work reported by Sathe et al.[39] The yield stress of PA6/PP blends also lies between neat PA6 and PP. Decrease in the yield strength indicates poor adhesion between the PA6 and PP as well.

Figure 4 shows the effect of PA6 and PP blending on the tensile strength and elongation at break. A similar trend to that of the yield stress can be observed here. The tensile strength of PA6 is higher than PP, supporting the finding that PA6 is "stronger" than PP. Thus, the incorporation of PP in PA6 will decrease the tensile strength of the latter.

When PA6 was subjected to tensile loading, plastic deformation and stable necking were observed. This is accompanied by a high elongation at break, compared to PP and PA6/PP blend, as indicated in Figure 4. Plastic deformation and necking were also found for the PP, albeit in lesser content compared to PA6. Thus, the elongation at break of PP is much lower than that of PA6. The PA6/PP blends showed an elongation at break that was lower than either PA6 or PP. No plastic deformation and necking was observed for the PA6/PP blend under tensile deformation. This may again be attributed to the poor adhesion between the PA6 matrix and minor PP dispersed therein. According to Sathe et al.,[39] in the PP/PA6 blends the components are incompatible, with almost no mutual adhesion. It is supposed that the large size of dispersed droplets hindered the cold drawing of PA6 and caused its premature rupture at low-elongation values. Note that PA6 and PP underwent necking, whereas all other PA6/PP blends showed no necking and thus a prominent decrease in ductility.[40]

The effect of blending of PA6 and PP on the flexural modulus and flexural strength is shown in Figure 5. In general, all materials displayed a similar trend to that observed in the tensile properties. The flexural properties of the PA6/PP blend lies between those of neat PA6 and PP. The addition of 30 wt % PP decreases the flexural modulus and flexural strength of PA6. A similar observation was also reported earlier by Sathe et al.[40] This indicates that no synergistic effect exists in respect to the mechanical properties when blending PA6 and PP. This fact is a further hint for the poor

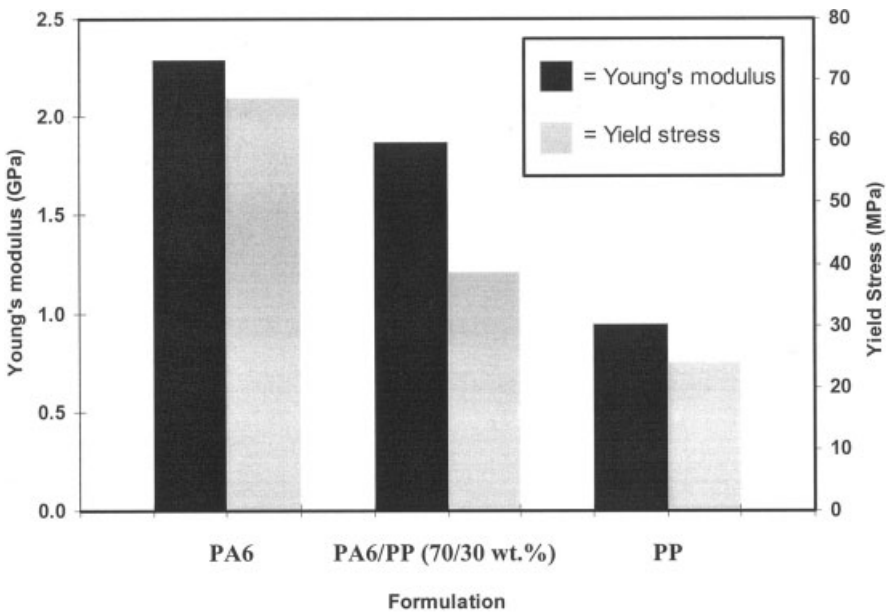

Figure 3 Effect of PA6 and PP blending on the Young's modulus and yield stress.

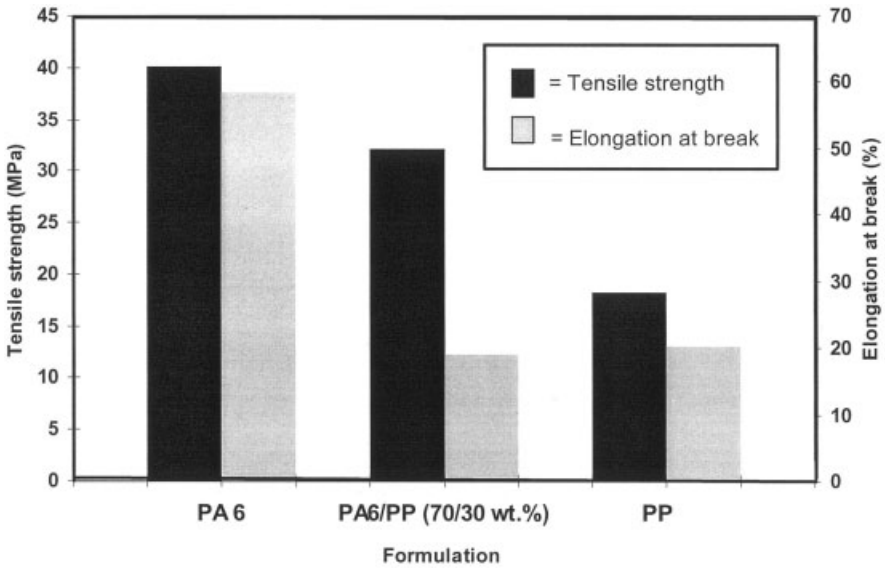

Figure 4 Effect of PA6 and PP blending on the tensile strength and elongation at break.

interaction between PA6 and PP. The PP droplets dispersed in the PA6 matrix act like "filled voids" because of the lacking interfacial adhesion. Accordingly, the loaded apparent cross section of the specimens is strongly reduced, which yield low-strength data.

Effect of organoclay loading

Figure 6 shows the effect of organoclay loading on the Young's modulus and tensile strength of PA6/PP blend. Note that Young's modulus increased monotonously with increasing organoclay content. The stiffness of the organoclay composites is markedly higher than that of the PA6/PP blend. Either full or partially delaminated clay formation is believed to be responsible for this behavior. The evidence for the clay exfoliation (delamination) will be provided later in this article. Earlier, Cho and Paul[12] reported that the modulus of PA6 composite containing 5 wt % of organoclay was substantially increased relative to neat PA6. Reichert et al.[6] also showed that the Young's modulus increased as a function of organophilic-layered silicates content. Shelley et al.[11] considered the possibility that the modulus improvements are due to the constraint of the polymer chains by their interaction with the clay surfaces. According to Huang et al.,[20] the introduction of the montmorillonite, which has a

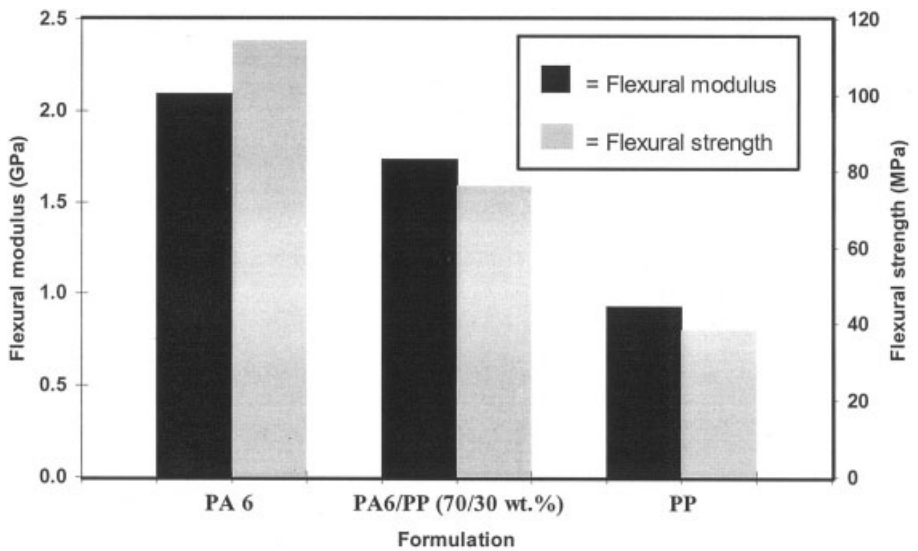

Figure 5 Effect of PA6 and PP blending on the flexural modulus and flexural strength.

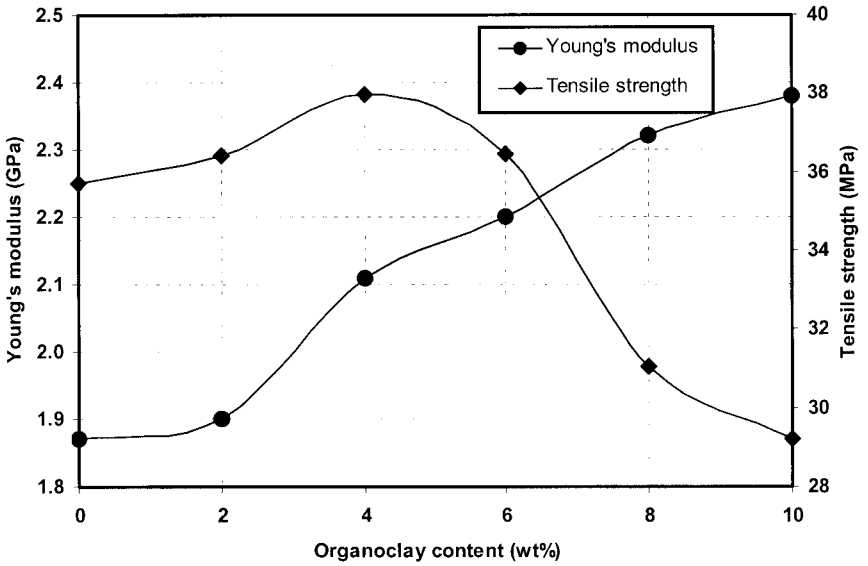

Figure 6 Effect of organoclay content on the Young's modulus and tensile strength of the blend PA6/PP (70/30 wt %).

higher modulus than the organosoluble PI matrix, leads to an increase in the modulus of the nanocomposite. The Young's modulus increased almost linearly up to 5 wt % of montmorillonite. However, as the montmorillonite content is further increased, the aggregation of the montmorillonite leads to a leveling off or even a slight decrease in the modulus of the hybrid. The addition of organoclay yields a substantial improvement in the stiffness of the composites based on PA6.[41]

The tensile strength increased until an optimum loading of organoclay is attained at 4 wt %. Further incorporation of organoclay reduced the strength gradually. It is believed that the tensile strength of organoclay-filled PA6/PP composites depends on several factors such as dispersion of the organoclay in the skin and core layers, interaction of PA6 with organoclay, compatibility of PA6 with PP, interaction of PP with organoclay, and filler–filler interaction of the organoclay.

A slight increase in the tensile strength of the PA6/PP blend with addition of organoclay (i.e., up to 4 wt %) may be due to the interaction of PA6 with the intercalant of the organoclay. Note that the amine groups of the modifier can react with the functional groups of the PA6 chains. The possible mechanism of interaction will be discussed in a subsequent publication. The high aspect ratio of organoclay may also increase the tensile strength by increasing the nanofiller contact surface with the polymer matrix. The tensile properties of organoclay-filled PA6/PP blend composites are also governed by the delamination of the organoclay, which is strongly dependent on the processing method and its condition. However, above an optimum loading (i.e., >4 wt % in the present study), the delamination of the organoclay is restricted. It is worth noting that the injection moldability of the PA6/PP blend based composites filled with more than 4 wt % organoclay became more difficult.

Another factor that possibly contributed to the lowering of tensile strength at high organoclay loading is the filler–filler interaction of organoclay, resulting in agglomerates. Agglomeration of organoclay yields a reduction of the aspect ratio of the organoclay and thus reduces the contact surface between organoclay and the polymer matrix. In addition, agglomeration of organoclay may also induce local stress concentrations in the composites. Thus, when subjected to tensile mode deformation, PA6/PP blend composite which contained higher loading of organoclay (i.e., 6 wt % and above) failed in a brittle manner, giving a relatively lower tensile strength. According to Huang et al.,[20] the tensile strength of organosoluble PI/montmorillonite hybrid increased with the montmorillonite content up to 6 wt % and then decreased thereafter. The strong interfacial interaction between the PI and montmorillonite improved the shear ability of the PI and increased the tensile strength of the hybrid.[20] As suggested by Akkapeddi,[42] there is a critical upper limit for clay to achieve the complete nanoscale exfoliation. Above a critical clay concentration, the clay aggregates persist.[42] According to Kornmann et al.,[27] the tensile strength of unsaturated polyester/montmorillonite nanocomposites is virtually unchanged but it decreases at a montmorillonite content of 10 vol %. A rough explanation for the onset of a threshold organoclay concentration is that the matrix molecules are less than needed to intermingle with those of the intercalant (modifier) of the clay. As a consequence,

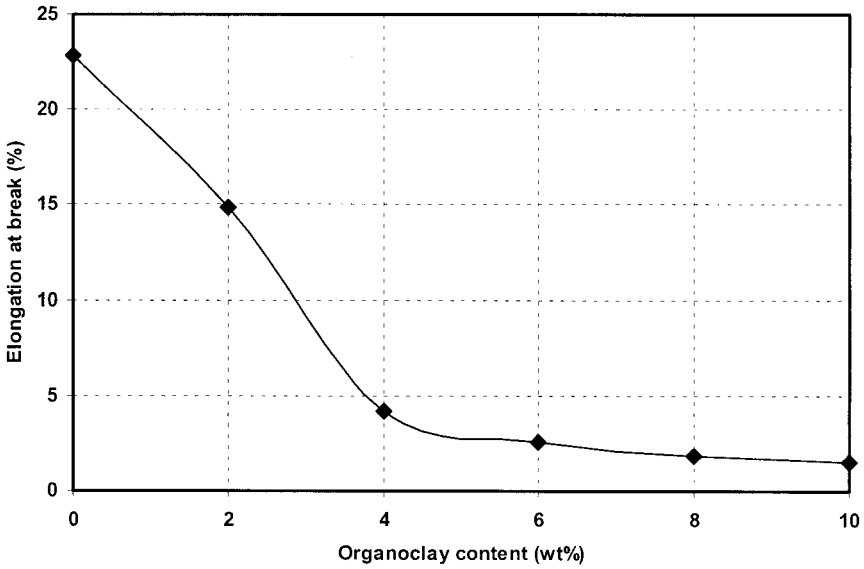

Figure 7 Effect of organoclay content on the elongation at break of the blend PA6/PP (70/30 wt %).

the clay layers are stacked together instead of their delamination.

The effect of organoclay loading on the elongation at break of PA6/PP composites is shown in Figure 7. The elongation at break decreased drastically with the incorporation of up to 4 wt % organoclay loading. The brittleness of these materials can be associated with the disappearance of plastic deformation of the polymer matrix as observed in the scanning electron microscopy. This subject will be discussed in detail later. Similar observation has been reported by Cho and Paul[12] and Reichert et al.[6] for nanocomposites based on PA6 and PP, respectively. A recent study on PA6 nanocomposites by Fornes et al.[41] indicates that, apart from strain rate, the brittleness of the material is also greatly affected by the molecular weight of PA6.

Figure 8 shows the effect of the organoclay loading on the flexural modulus and flexural strength of PA6/PP composites. A similar trend to that of Young's modulus (shown in Fig. 6) can be observed. The flexural modulus of organoclay-filled PA6/PP composites increased by increasing the organoclay loading. Not much change in the flexural strength can be observed with the incorporation of up to 10 wt % of organoclay into the PA6/PP blend. However, it is interesting to note that the flexural strength of the composites reached an optimum value at 4 wt % loading of organoclay. Beyond that, the strength of the

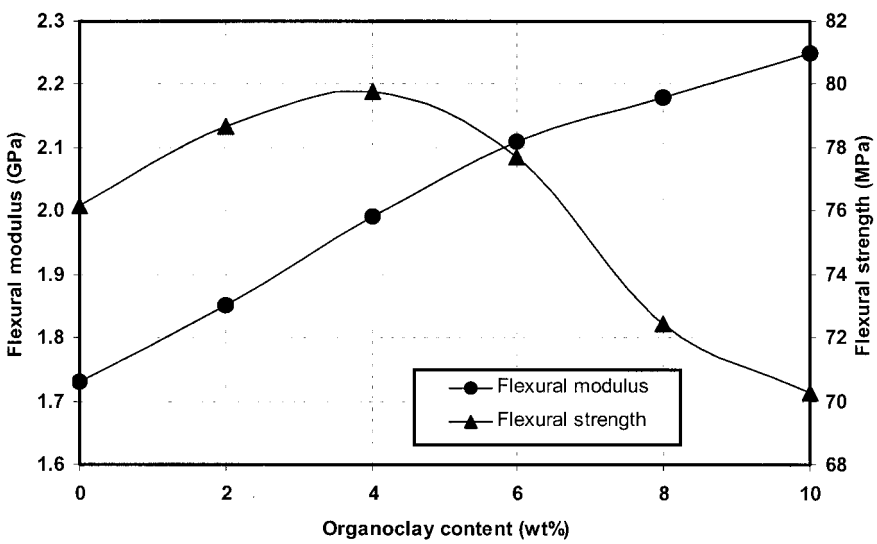

Figure 8 Effect of organoclay on the flexural modulus and strength of the blend PA6/PP (70/30 wt %).

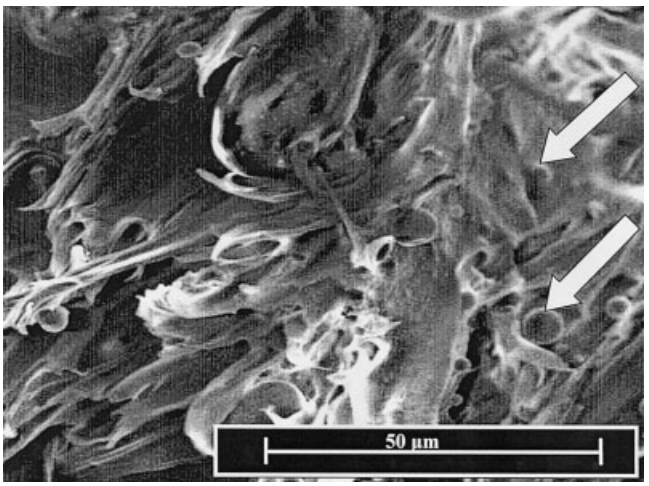

Figure 9 SEM micrograph showing the tensile fracture surface of a PA6/PP (70/30 wt %) blend.

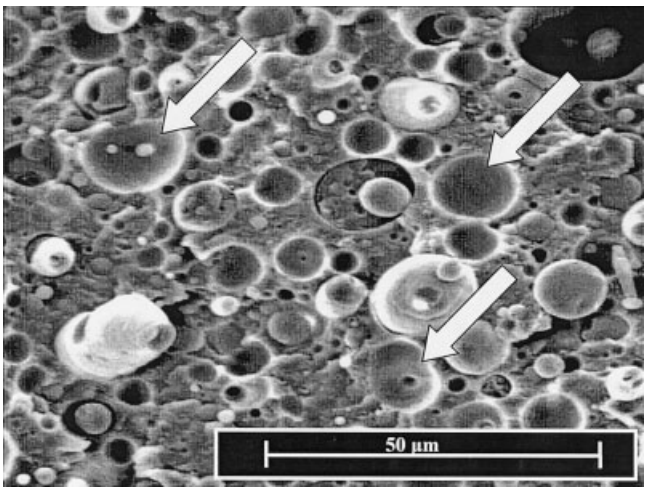

Figure 10 SEM micrograph showing the tensile fracture surface of a 4 wt % organoclay-filled PA6/PP composite.

composites dropped gradually until it became even lower than the strength of neat PA6/PP blend. This trend is in agreement with the results on the tensile strength (cf. Fig. 6).

As mentioned earlier, mechanical properties of organoclay-filled PA6/PP composites are dependent on the dispersion of the organoclay particles, their orientation in the skin and core layers, and their exfoliation degree. Recall that the organoclay has a platelike structure irrespective to its exfoliation degree. According, the platy organoclay and its layers when exfoliated are aligned in the mold fill direction (MFD).[11] This alignment may cause the observed increase in the flexural strength. According to Kim et al.,[43] the injection-molding direction is parallel to the long axis of the layered silicates. This forced orientation is a result of the high shear rates during injection molding. On the other hand, in the central section of the injection-molded specimens, the agglomerated clay particles should be oriented transverse to the MFD based on the analogy with short fiber-reinforced composites. Note that in the central zone small elongational forces prevail, which support the clay exfoliation less.

At higher organoclay loading, the agglomerated organoclay particles possibly acted as stress concentration sites. This likely caused premature failure and was associated with a reduction of the flexural strength values. Another interesting point worth mentioning is that the flexural strength of PA6/PP nanocomposites was markedly higher than the tensile one, irrespective of the organoclay loading. A similar observation has also been reported by Liu et al.,[44] for PA6 nanocomposites filled with 5 wt % montmorillonite clay. The flexural strength and tensile strength data are 139 and 89 MPa, respectively. However, no further explanation was forwarded for the observed data. This large difference is likely an effect of the molding-induced skin-core morphology. In the skin layers, the clay layers are aligned in the MFD and well exfoliated. Note that the skin layers are under tension/compression forces during the flexural tests and the orientation of the clay layers is favorable. On the other hand, in core agglomerated clay particles are mostly present, which are not only less favorably oriented to suffer tensile loading but also work as stress concentrators. This is the reason for low ductility and premature failure.

Effect of organoclay loading on the morphology

Little has been published that discussed the fracture surface morphology of polymer nanocomposites by using SEM. It is known that SEM is not a suitable technique to characterize the morphology of polymer nanocomposites. However, in the present study, SEM analysis

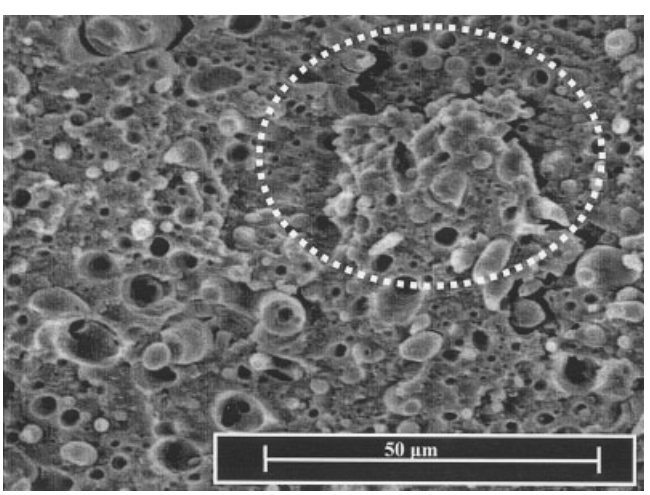

Figure 11 SEM micrograph showing the tensile fracture surface of a 6 wt % organoclay-filled PA6/PP composite.

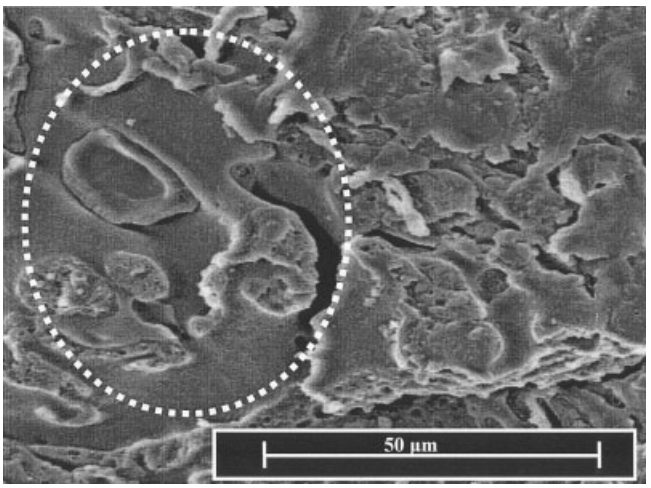

Figure 12 SEM micrograph photograph showing the tensile fracture surface of a 10 wt % organoclay-filled PA6/PP composite.

was used to investigate the effect of the organoclay on the tensile fractured surface morphology of PA6/PP blend nanocomposites. Emphasis was to clarify the ductile–brittle transition in the PA6/PP blends when filled with organoclay. Further evidence on the exfoliation of PA6/PP nanocomposites will be provided by TEM analysis, reported later in this section.

Figure 9 shows the SEM micrograph of the tensile fractured surface of neat PA6/PP blends. The PP droplets formed are shown by white arrows. They induce some cavitation of the PA6 because of which a fibrillar PA6 structure appears. The incompatibility of the PA6 and PP blends could be observed through the PA6 fibril structure and the PP droplet morphology. The SEM micrograph of tensile fractured surface of 4 wt % organoclay-filled PA6/PP composites is shown in Figure 10. The fibrillated morphology observed in the neat PA6/PP blend (cf. Fig. 9) disappeared in this case. However, the presence of PP droplets that were detached from the PA6 matrix is very obvious on the fracture plane (shown by the white arrows). The absence of fibrillated structure is a direct manifestation of the missing plastic deformation of PA6 matrix (embrittlement) due to the incorporation of the organoclay. This explains the low elongation at break, or brittleness displayed by PA6/PP nanocomposites at $\geq$4 wt % organoclay loading (cf. Fig. 7). Figure 11 shows the SEM micrograph of tensile fractured surface of 6 wt % organoclay-filled PA6/PP composites. The PP droplets that were detached from the PA6 matrix can still be well resolved. Besides, a "microcrack" can be seen on the fracture plane (shown in the white dotted line circle). This may be attributed to the agglomeration or the enrichment of the organoclay, which likely occurred in the PA6 instead of the PP phase. A more pronounced morphological transformation can be observed for the PA6/PP nanocomposites filled with 10 wt % organoclay (cf. Fig. 12). Neither a fibrillated morphology nor PP droplets detached

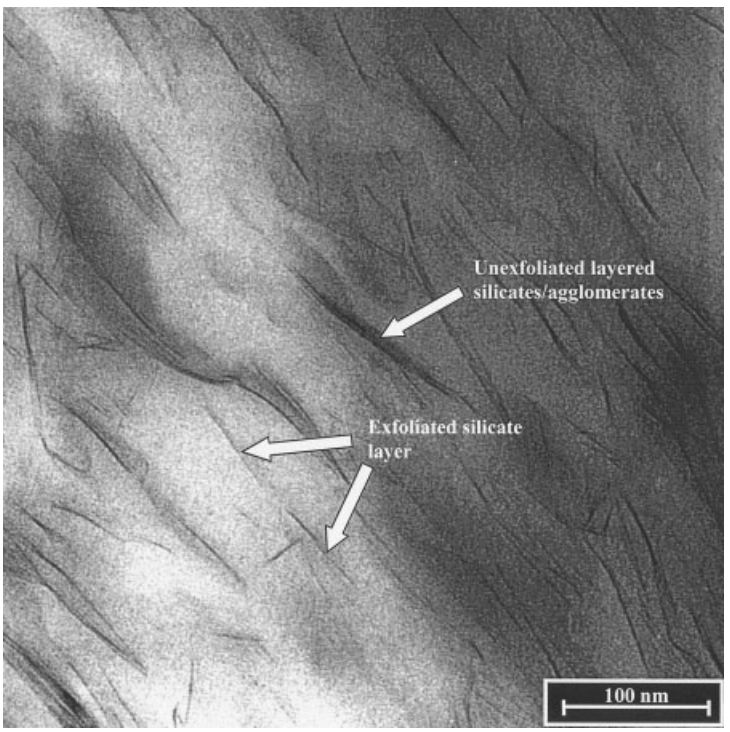

Figure 13 TEM micrograph taken from the PA6/PP nanocomposites containing 4 wt % organoclay.

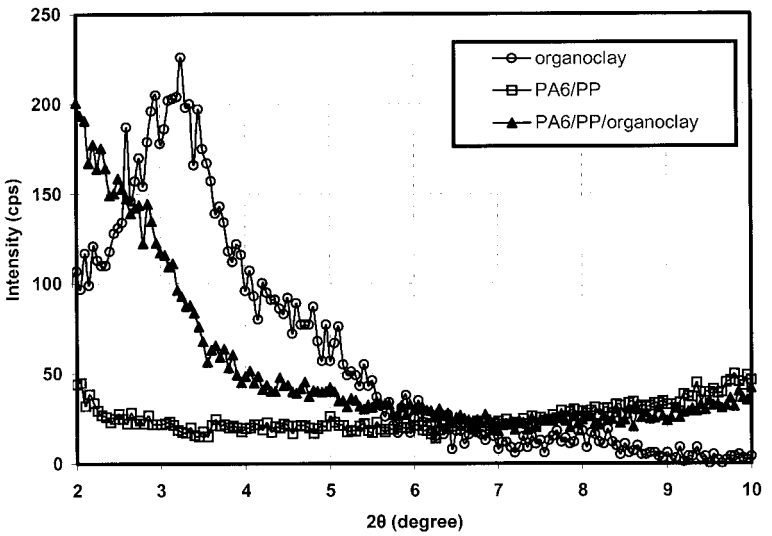

Figure 14 XRD patterns for organoclay, PA6/PP blend, and PA6/PP nanocomposites containing 4 wt % organoclay.

from the PA6 matrix could be observed here. The presence of microcracking (shown in the white circle) caused by stress concentration sites (i.e., agglomerated particles) provide good evidence for the brittleness of the material. In addition, the onset of microcracking is traced for the drop in the strength of the organoclay-filled PA6/PP composites. Accordingly, the organoclay is supposed to be preferentially embedded in the PA6 phase.

A TEM micrograph of the PA6/PP nanocomposites containing 4 wt % of organoclay is shown in Figure 13. The dark lines represent the thickness of individual clay layers or agglomerates. The average thickness of the clay platelets appears to be just a few nanometers, whereas the average length is about 100 nm. The organoclay was oriented in the MFD as expected. The darker lines show stacked silicate layers due to clustering or agglomeration. Similar results were also re-

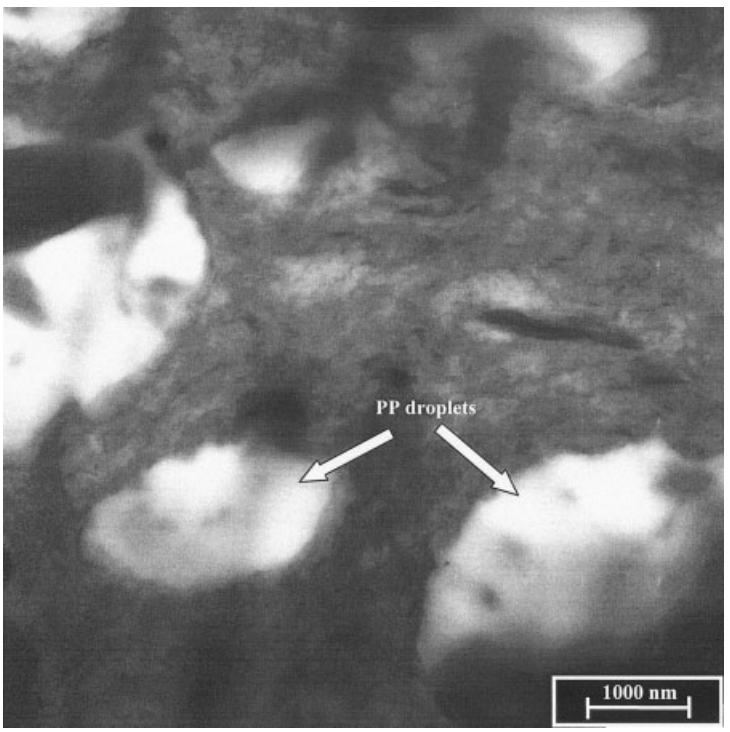

Figure 15 TEM micrograph showing the distribution of the organoclay and PP in the PA6/PP nanocomposites.

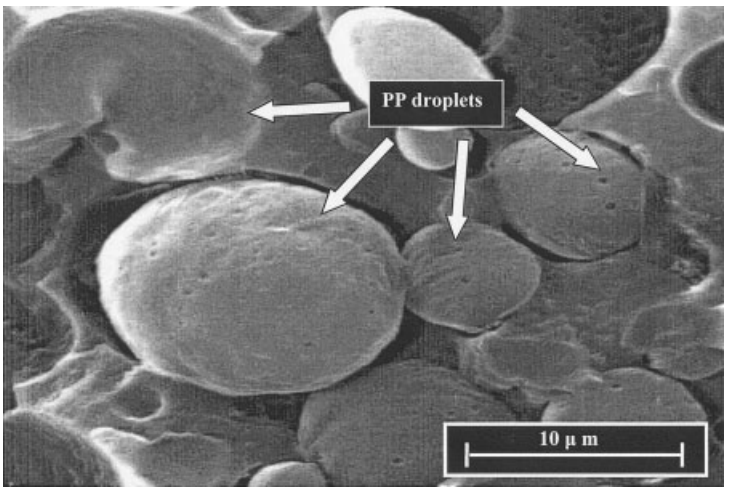

Figure 16 SEM micrograph taken from the surface of an unetched PA6/PP/organoclay nanocomposites (70/30/4 wt %).

ported by other works for other nanocomposite. An earlier work done by Cho and Paul[12] showed that organoclay is well exfoliated in the PA6 matrix and the individual layers are aligned to the flow axis. According to Akkapeddi,[42] the high-melt viscosity of PA6 generates high-shearing stresses on the clay platelets stacks, locally causing a progressive delamination and exfoliation (i.e., formation of individual platelets from the aggregated structure).

XRD characterization

Figure 14 shows the XRD patterns for organoclay and PA6/PP nanocomposites. The results of XRD patterns is in the range of $2\theta = 2$–$10°$. The organoclay patterns reveal a broad intense peak at around $2\theta = 3.25°$, corresponding to a basal spacing of 2.72 nm. The XRD pattern of organoclay-filled PA6/PP does not show a characteristic basal reflection of the pristine organoclay. This provides further evidence to that derived from the TEM for the formation of an exfoliated structure. However, the degree of exfoliation could not be established here, and further experimental work has to be performed to prove it. Wu et al.[45] have reported a similar observation in the case of PA 1012/clay nanocomposites. The absence of the characteristic clay d_{001} peak indicated the exfoliation of the clay in the PA1012 matrix. The absence of the characteristic clay d_{001} peak in a PA6/organoclay is evidence for the formation of an exfoliated nanocomposite.[12] According to Hsiao et al.,[19] the silicate layers of dodecyl ammonium exchange montmorillonite were exfoliated in the PI because the characteristic clay peaks did not appear in the related XRD diffractograms. Yano et al.[21] also reported that PI/organophilic montmorillonite hybrid showed no peak in the XRD diffraction traces

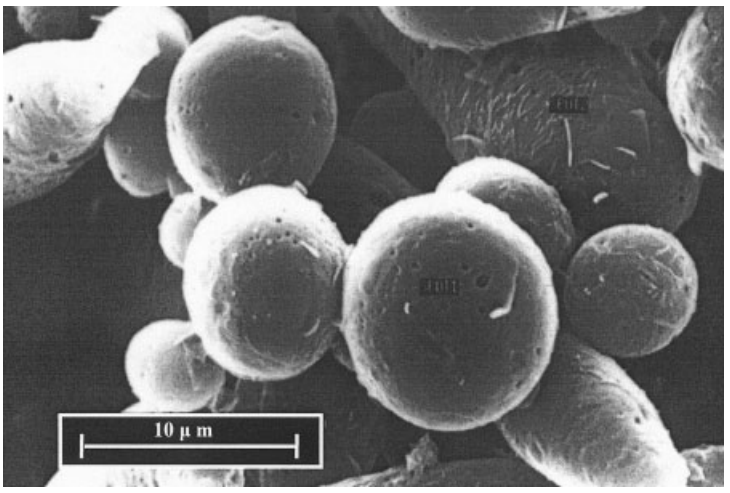

Figure 17 SEM micrograph taken from the surface of a formic acid etched PA6/PP nanocomposites containing 4 wt % organoclay.

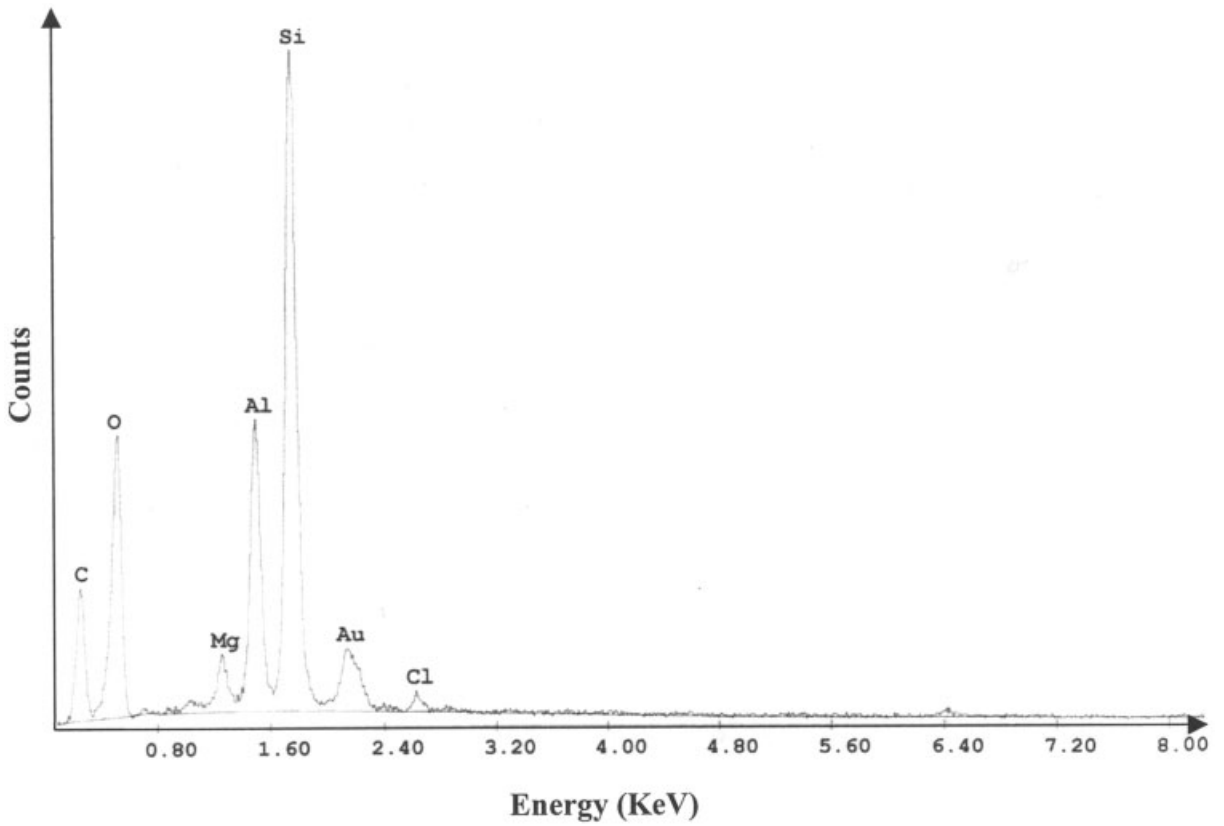

Figure 18 EDX spectrum of the organoclay with ammonium intercalant (C18).

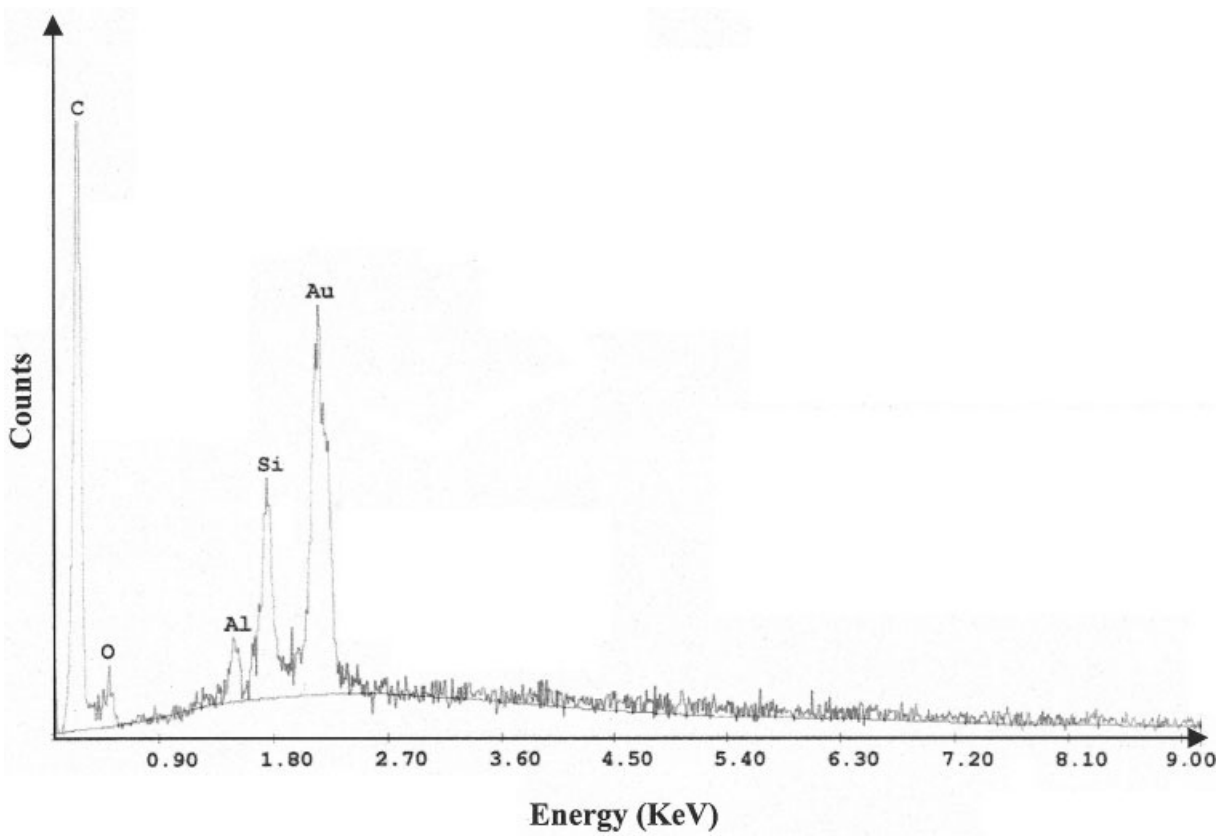

Figure 19 EDX spectrum of an unetched PA6/PP nanocomposites containing 4 wt % organoclay.

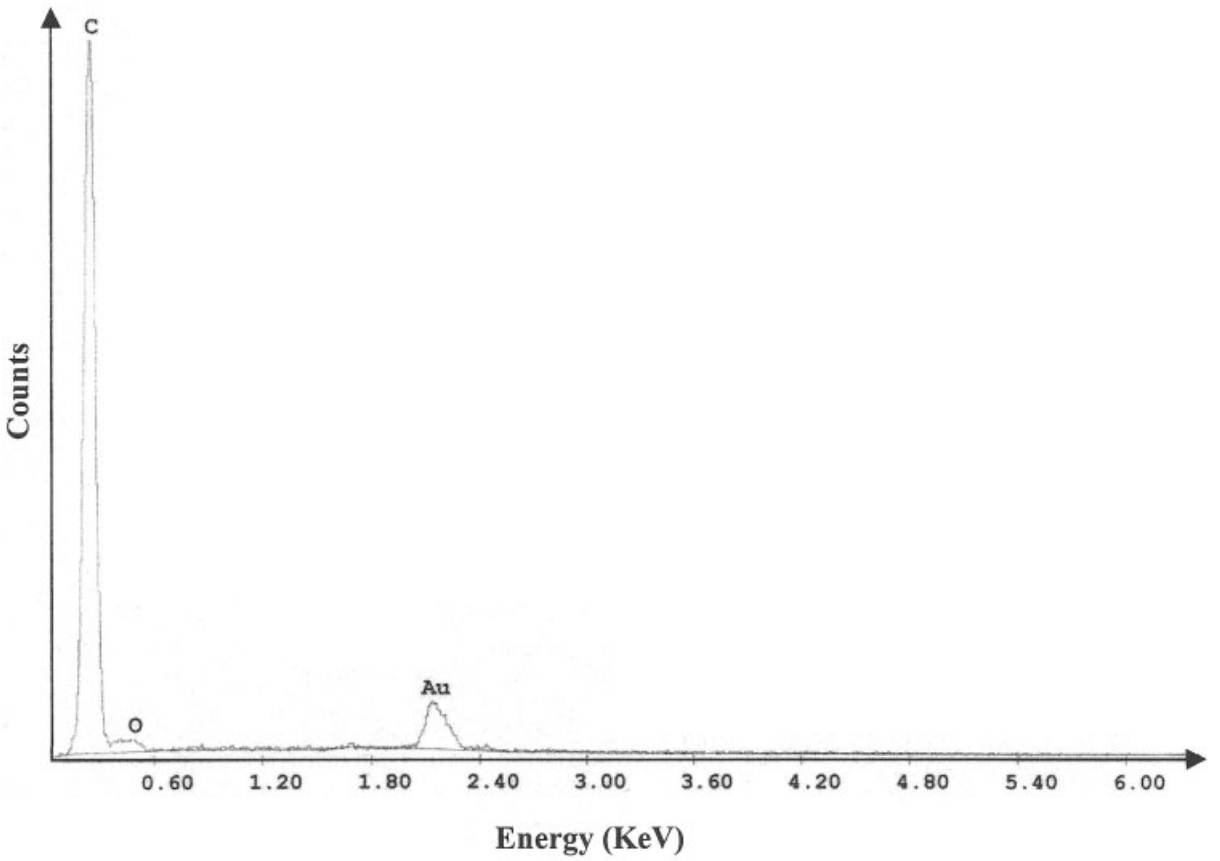

Figure 20 EDX spectrum of a formic acid etched PA6/PP nanocomposites containing 4 wt % organoclay.

ranging from $2\theta = 2°$ to $2\theta = 10°$. This revealed that organophilic montmorillonite in the PI matrix was exfoliated completely (i.e., dispersed homogeneously).

Location of the organoclay

In this study, evidence obtained from the TEM, SEM, and energy-dispersion X-ray analysis (EDX) techniques will be used to determine the location of the organoclay in PA6/PP nanocomposites. It can be anticipated that the organoclay has a much higher affinity to PA6 phase because of the possible interaction listed above than to the PP. According to Akkapeddi,[42] the organic intercalant in the clay plays the role of a dispersion aid by weakening the interlayer adhesion and promoting the compatibility with the PA chains via strong polar interactions.

The distribution of the organoclay in the PA6/PP nanocomposites is shown by the TEM picture in Figure 15. The large and white particles are PP droplets, whereas the PA6 appears as a gray background. Most of the dark lines which represent clay can be resolved in the gray background. This indicates that the organoclay has a strong tendency to be located in the PA6 phase. Figures 16 and 17 show the SEM micrograph of the unetched and formic acid etched surface of PA6/PP nanocomposites containing 4 wt % organoclay. The former picture shows the presence of large PP particles distributed in the PA6 matrix, whereas the latter one shows the residual PP particle after PA6 phase was removed by formic acid. When formic acid was added to PA6/PP blends, the PA6 was dissolved completely within 1–3 h.[39]

Figure 18 shows the EDX spectra of the organoclay in the as received state. Five elements were detected, C, O, Mg, Al, and Si. The carbon (C) was observed in the EDX because of the octadecylamine intercalant. Recall that the used organoclay contained montmorillonite clay (70–85 wt %) and octadecylamine (15–30 wt %). The Au element observed in the EDX is associated with the coating (gold) used to avoid charging of the sample. EDX spectra of both unetched and etched samples provided spectra as shown in Figures 19 and 20, respectively. For the unetched PA6/PP nanocomposites (cf. Fig. 19), four elements, C, O, Si, and Al, were detected. The presence of the Si indicates that organoclay was distributed in the PA6/PP matrix. Interestingly, when the EDX spectra were taken of the residue after formic acid etching (i.e., PP), only C and O elements could be detected. The absence of the Si suggests that the organoclay was located entirely in the PA6 phase. When the PA6 was etched away by

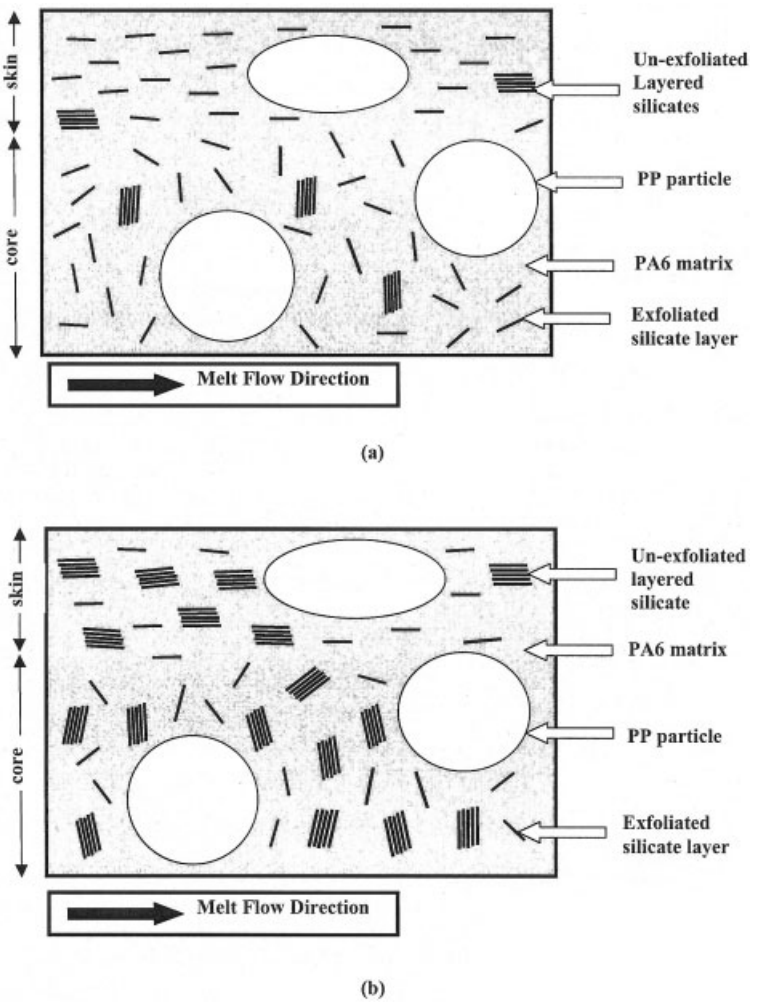

Figure 21 (a) Schematic sketch for the proposed morphology of PA6/PP nanocomposites containing 4 wt % organoclay or less. (b) Schematic sketch for the proposed morphology of PA6/PP nanocomposites containing more than 4 wt % organoclay.

formic acid, the organoclay was also removed. Accordingly, the organoclay must have been located in the PA6 phase. Nevertheless, further research is currently in progress to ascertain this issue.

Figure 21(a) shows a schematic representation of the morphology of the PA6/PP nanocomposites containing 4 wt % organoclay. This scheme is made on the basis of the collective findings derived from TEM, SEM, EDX, and XRD techniques. The proposed morphology shows exfoliated silicate layers distributed in the PA6 phase. However, some unexfoliated layered silicates/agglomerates also coexist in the PA6 phase (indicated by the white arrows). The PP particles were elongated in the skin layer but more spherical particles were resolved in the core layer, in agreement with the work done by Karger-Kocsis and Csikai.[46] The organoclay layers and aggregates are aligned in the skin along the MFD and more randomly or even transversely in the core layer. This is in analogy to the structure of short fiber-reinforced injection-molded system. The extent of the unexfoliated layered silicates/agglomerates can be expected to be higher when the organoclay loading increased beyond 4 wt %. Figure 21(b) shows the schematic representation on the morphology of the PA6/PP nanocomposites containing more than 4 wt % of organoclay.

CONCLUSION

Based on this study devoted to study the mechanical properties and morphology of an injection-molded PA6/PP blend (70/30 wt %) reinforced by organophilic layered clay (organoclay), the following conclusions can be drawn.

Mechanical properties

A good balance between stiffness, strength, and toughness (ductility) was achieved at 4 wt % organoclay content. The flexural strength was twofold of the tensile one, which was attributed to the effect of the injection molding induced skin-core structure and the

alignment of the exfoliated/agglomerated organoclay therein. Increasing of organoclay content resulted in a severe embrittlement manifested in a drop of the tensile elongation at break. This was traced to the enrichment of organoclay in the PA6 phase, making it brittle.

Morphology

The minor PP phase was present in the form of large particles in the PA6 matrix. The interfacial adhesion between PA6 and PP was very poor. XRD results show that the organoclay is exfoliated (delaminated). TEM and EDX analysis of selectively etched samples (the PA6 phase was removed by formic acid) evidenced that the organoclay is exclusively present in the PA6 phase.

The authors thank the Ministry of Science, Technology, and Environment (MOSTE), Malaysia for the IRPA grant (063171/IRPA Jangka Panjang). A special scholarship, granted by Universiti Sains Malaysia to one of us (C.W.S.), is gratefully acknowledged.

References

1. Zanetti, M.; Lomakin, S.; Camino, G. Macromol Mater Eng 2000, 279, 1.
2. Lan, T.; Liang, Y.; Beall, G. W.; Kamena, K. Advances in Nanomer ® Additives for Clay/Polymer Nanocomposites; Additives '99; San Francisco, 1999.
3. Lee, J. W.; Lim, Y. T.; Park, O. O. Polym Bull 2000, 45, 191–198.
4. Wang, H.; Elkovitch, M.; Lee, L. J.; Koelling, K. W. ANTEC 2000: Processing and Properties of Polymer Nano-Composites; 2000.
5. Kawasumi, M.; Hasegawa, N.; Kato, M.; Usuki, A.; Okada, A. Macromolecules 1997, 30, 6333.
6. Reichert, P.; Nitz, H.; Klinke, S.; Brandsch, R.; Thomann, R.; Mülhaupt, R. Macromol Mater Eng 2000, 275, 8.
7. Hambir, S.; Bulakh, N.; Kodgire, P.; Kalgaonkar, R.; Jog, J. P. J Polym Sci, Part B: Polym Phys 2001, 39, 446.
8. Reichert, P.; Hoffmann, B.; Bock, T.; Thomann, R.; Mülhaupt, R.; Friedrich, C. Macromol Rapid Commun 2001, 22, 519.
9. Solomon, M. J.; Almusallam, A. S.; Seefeldt, K. F.; Somwangthanaroj, A.; Varadan, P. Macromolecules 2001, 34, 1864.
10. Zanetti, M.; Camino, G.; Reichert, P.; Mülhaupt, R. Macromol Rapid Commun 2001, 22, 176.
11. Shelley, J. S.; Mather, P. T.; DeVries, K. L. Polymer 2001, 42, 5849.
12. Cho, J. W.; Paul, D. R. Polymer 2001, 42, 1083.
13. Kojima, Y.; Usuki, A.; Kawasumi, M.; Okada, A.; Kurauchi, T.; Kamigaito, O. J Polym Sci, Part A: Polym Chem 1993, 31, 983.
14. Fong, H.; Vaia, R. A.; Sanders, J. H.; Lincoln, D.; John, P. J.; Vreugdenhil, A. J.; Bultman, J.; Cerbus, C. A.; Jeon, H. G. Polym Prepr 2001, 42, 354.
15. Lincoln, D. M.; Vaia, R. A. Polym Prepr 2001, 42, 55.
16. Sikka, M.; Cerini, L. N.; Ghosh, S. S.; Winey, K. I. J Polym Sci, Part B: Polym Phys 1996, 34, 1443.
17. Hoffmann, B.; Dietrich, C.; Thomann, R.; Friedrich, C.; Mülhaupt, R. Macromol Rapid Commun 2000, 21, 57.
18. Park, C. I.; Park, O. O.; Lim, J. G.; Kim, H. J. Polymer 2001, 42, 7465.
19. Hsiao, S. H.; Liou, G. S.; Chang, L. M. J Appl Polym Sci 2001, 80, 2067.
20. Huang, J. C.; Zhu, Z. K.; Ma, X. D.; Qian, X. F.; Yin, J.; J Mater Sci 2001, 36, 871.
21. Yano, K.; Usuki, A.; Okada, A.; Kurauchi, T.; Kamigaito, O. J Polym Sci, Part A: Polym Chem 1993, 31, 2493.
22. Chin, I. J.; Thurn-Albrecht, T.; Kim, H. C. Polym Prepr 2000, 41, 591.
23. Curliss, D. B. Polym Prepr 2000, 41, 523.
24. Kornmann, X.; Lindberg, H.; Berglund, L. A. Polymer 2001, 42, 1303.
25. Jiang, G. J.; Tsai, H. Y. Polym Prepr 2000, 41, 621.
26. Huang, X. Y.; Brittain, W. J. Polym Prepr 2000, 41, 521.
27. Kornmann, X.; Berglund, L. A.; Sterte, J.; Giannelis, E. P. Polym Eng Sci 1998, 38, 1351.
28. Jimenez, G.; Ogata, N.; Kawai, H.; Ogihara, T. J Appl Polym Sci 1997, 64, 2211.
29. Choi, H. J.; Kim, S. G.; Hyun, Y. H.; John, M. S. Polym Prepr 2000, 41, 1183.
30. Huang, X. Y.; Lewis, S.; Brittain, W. J.; Vaia, R. A. Polym Prepr 2000, 41, 589.
31. Holsti-Miettinen, R. M.; Perttila, K. P.; Seppala, J. V.; Heino, M. T. J Appl Polym Sci 1995, 58, 1551.
32. Kojima, Y.; Usuki, A.; Kawasumi, M.; Okada, A.; Kurauchi, T.; Kamigaito, O. J Appl Polym Sci 1993, 49, 1259.
33. Ide, F.; Hasegawa, A. J Appl Polym Sci 1974, 18, 963.
34. Liang, B. R.; White, J. L.; Spruiell, J. E.; Goswami, B. C. J Appl Polym Sci 1983, 28, 2011.
35. Fried, J. R. Polymer Science and Technology; Prentice Hall: New York, 1995; p 271.
36. Marco, C.; Ellis, G.; Gómez, M. A.; Fatou, J. G.; Arribas, J. M.; Campoy, I.; Fontecha, A. J Appl Polym Sci 1997, 65, 2665.
37. Park, S. J.; Kim, B. K.; Jeong, H. M. Eur Polym J 1990, 26, 131.
38. Robson, P.; Sandilands, G. J.; White, J. J Appl Polym Sci 1981, 26, 3515.
39. Sathe, S. N.; Devi, S.; Srinivasa Rao, G. S.; Rao, K. V. J Appl Polym Sci 1996, 61, 97.
40. Sathe, S. N.; Srinivasa Rao, G. S.; Rao, K. V.; Devi, S. Polym Eng Sci 1996, 36, 2443.
41. Fornes, T. D.; Yoon, P. J.; Keskkula, H.; Paul, D. A. Polymer 2001, 42, 9929.
42. Akkapeddi, M. A. Polym Composites 2000, 21, 576.
43. Kim, G. M.; Lee, D.-H.; Hoffmann, B.; Kressler, J.; Stöppelmann, G. Polymer 2001, 42, 1095.
44. Liu, X.; Wu, Q.; Berglund, L. A.; Fan, J.; Qi, Z. Polymer 2001, 42, 8235.
45. Wu, Z.; Zhou, C.; Qi, R.; Zhang, H. J Appl Polym Sci 2002, 83, 2403.
46. Karger-Kocsis, J.; Csikai, I. Polym Eng Sci 1987, 27, 241.